A&A 422, 97–102 (2004)
DOI: 10.1051/0004-6361:20040291

Astronomy & Astrophysics

Simultaneous X-ray and ultraviolet spectroscopy of the Seyfert galaxy NGC 5548

III. X-ray time variability

J. S. Kaastra[1], K. C. Steenbrugge[1], D. M. Crenshaw[2], S. B. Kraemer[3,4], N. Arav[5], I. M. George[6,7], D. A. Liedahl[8], R. L. J. van der Meer[1], F. B. S. Paerels[9], T. J. Turner[6,7], and T. Yaqoob[7,10]

[1] SRON National Institute for Space Research, Sorbonnelaan 2, 3584 CA Utrecht, The Netherlands, USA
[2] Department of Physics and Astronomy, Georgia State University, Astronomy Offices, One Park Place South SE, Suite 700, Atlanta, GA 30303, USA
[3] Catholic University of America, USA
[4] Laboratory for Astronomy and Solar Physics, NASA's Goddard Space Flight Center, Code 681, Greenbelt, MD 20771, USA
[5] CASA, University of Colorado, 389 UCB, Boulder, CO 80309-0389, USA
[6] Joint Center for Astrophysics, University of Maryland, Baltimore County, 1000 Hilltop Circle, Baltimore, MD 21250, USA
[7] Laboratory for High Energy Astrophysics, Code 660, NASA's Goddard Space Flight Center, Greenbelt, MD 20771, USA
[8] Physics Department, Lawrence Livermore National Laboratory, PO Box 808, 41, Livermore, CA 94550, USA
[9] Columbia Astrophysics Laboratory, Columbia University, 538W. 120th Street, New York, NY 10027, USA
[10] Department of Physics and Astronomy, Johns Hopkins University, Baltimore, MD 21218, USA

Received 18 February 2004 / Accepted 12 April 2004

Abstract. The Seyfert 1 galaxy NGC 5548 was observed for a week by Chandra using both the HETGS and LETGS spectrometers. In this paper we study the time variability of the continuum radiation. During our observation, the source showed a gradual increase in flux over four days, followed by a rapid decrease and flattening of the light curve afterwards. Superimposed upon these relatively slow variations several short duration bursts or quasi-periodic oscillations occured with a typical duration of several hours and separation between 0.6–0.9 days. The bursts show a delay of the hard X-rays with respect to the soft X-rays of a few hours. We interpret these bursts as occurring due to a rotating, fluctuating hot spot at approximately 10 gravitational radii; the time delay of the hard X-rays from the bursts agrees with the canonical picture of Inverse Compton scattering of the soft accretion disk photons on a hot medium that is relatively close to the central black hole.

Key words. galaxies: active – galaxies: Seyfert – galaxies: individual: NGC 5548 – X-rays: individual: NGC 5548 – X-rays: galaxies

1. Introduction

Active Galactic Nuclei (AGN) are well-known for their violent environment. Gas is being swallowed by the black hole, fed by a continuous supply of fresh material through an accretion disk. This process becomes visible as intense high-energy radiation from the disk and its immediate surroundings, in particular close to the black hole. This radiation field may drive outflows from the nucleus. The detection of these outflows gives us a way to probe into the inner nuclear regions.

Recent high-resolution X-ray spectra, starting with the first observation of the Seyfert 1 galaxy NGC 5548 (Kaastra et al. 2000) and high-resolution UV spectra (Crenshaw & Kraemer 1999; Kriss et al. 2000), allowed for an unprecedented study of the ionization and dynamical structure of the outflowing photoionized winds. In the framework of a study of these winds, we proposed to re-observe NGC 5548 in order to obtain simultaneous high-resolution, high signal-to-noise X-ray and UV spectra.

NGC 5548 was observed for a full week with Chandra in January 2002 using both the High Energy Transmission Grating Spectrometer (HETGS) and Low Energy Transmission Grating Spectrometer (LETGS), with simultaneous UV observations taken by the Space Telescope Imaging Spectrograph (STIS). The analysis of the warm absorber is presented elsewhere (UV spectra: Paper I, Crenshaw et al. 2003; X-ray spectra: Paper II, Steenbrugge et al. 2004). Limits to the spatial extent of the X-ray source were discussed by

Send offprint requests to: J. S. Kaastra,
e-mail: J.S.Kaastra@sron.nl

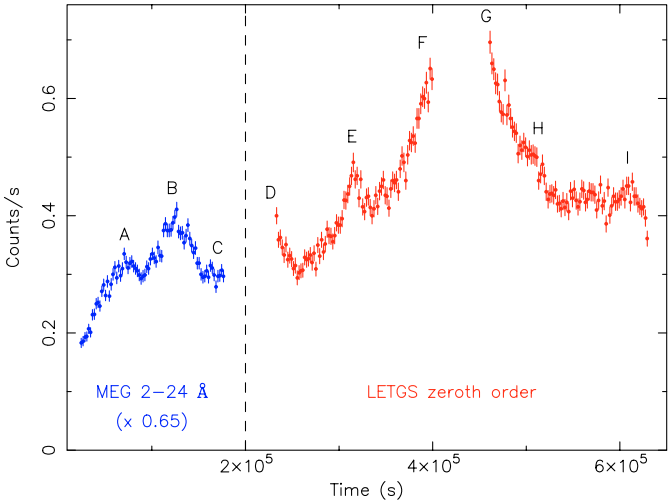

Fig. 1. X-ray light curve of NGC 5548. The data have been binned in bins of 2000 s. Times in this and all subsequent figures are measured relative to MJD 52290 (Jan. 16, 2002, time 00:00:00). The two data gaps are caused by the perigee passage of *Chandra*. The left part of the plot contains the 2–24 Å count rate as measured with the MEG in +1 and −1 order combined, multiplied by a factor of 0.65 in order to be at approximately the same scale as the zeroth order count rate with the LETGS (middle and right part). We estimate the uncertainty in this scale factor as ∼10%. Capitals indicate the peaks discussed in the text.

Kaastra et al. (2003). In this paper we discuss the continuum time variability of the source during this observation.

2. Observations and data extraction

The present observation of NGC 5548 was obtained in January 2002. The observation was split over three orbits of the Chandra satellite. In the first orbit (151 ks exposure time, start January 16, 2002) the HETG/ACIS-S configuration was used, in the second (170 ks exposure, start January 18) and third (171 ks exposure, start January 21) the LETG/HRC-S configuration was used. The HETGS data were reduced using the standard CIAO software version 2.0b. The LETGS data were reduced using dedicated software as described in Kaastra et al. (2002). The combined observation spans a time interval of a full week. All times reported in this paper are given in seconds relative to MJD 52290 (Jan. 16, 2002, time 00:00:00).

3. Time variability

3.1. Light curve

We constructed the LETGS zeroth order light curve of NGC 5548 by extracting all events within a radius of 100 pixels from the location of the source. The background, estimated from a nearby region, is negligible as compared to the flux of the source, and shows no significant time variations. Note that due to the use of the HRC-S detector, pile-up in the zeroth order can be neglected.

Figure 1 shows the light curve extracted from the zeroth order of the LETGS, combined with the first order MEG count rate, scaled to approximately the corresponding LETGS level. We estimate the uncertainty in this scaling factor to be ∼10%, taking into account the absolute calibration uncertainties of both instruments (in particular the zeroth order effective area of the LETGS). The light curve is characterized by a rise during four days from 0.2 to 0.7 c/s, with superimposed short duration (few hours) fluctuations. The characteristic exponential rise time toward the peak at t = 400 ks is a few days followed by a decay with a similar time scale up to t = 520 ks. After that time, the light curve remains approximately constant for a day till the end of the observation.

The light curve also exhibits a few peaks, which we call here "bursts", and which are labeled with the letters A through I in Fig. 1. The clearest example is the burst which reaches its maximum at t = 314.2 ± 1.1 ks and lasts for about 20 ks (labeled "E" in Fig. 1). Its peak amplitude is about 0.092 ± 0.010 c/s above the underlying rising flux of 0.369 c/s, i.e. an increase of 25% of this steadily rising flux level.

We note that bursts A, B and C are not only present in the MEG data, but are also visible in the HEG data as well as the zeroth-order light curve of the HETGS. This zeroth-order light curve, due to the use of the ACIS detector, has strong pile-up effects that make it less useful for quantitative analysis. Therefore we concentrate here on the MEG first order data. The combined light curves also show evidence for two very prominent short-lived bursts at either side of burst B.

While bursts A, B and E are clearly recognizable in Fig. 1, the others are less obvious. Here we present our arguments why we think these other bursts are significant. It is evident that the light curve has a local maximum between burst C and D. Instead of two or more separate bursts the data would also be consistent with a single peak during this interval. However, the spectral variability (see Sect. 3.2) indicates a similar behavior at point C as at the start of the better observed bursts: a maximum in the soft flux while the hard flux is still rising (Fig. 3). Therefore we tentatively assume that there are two bursts, C and D, bracketing the perigee passage (the instrumental background is small so this is not an artifact induced by the Chandra orbit). Also, D is similar to the start of E (see Figs. 2 and 4). This last figure shows the same type of "hysteresis" for burst D (sequence 1–6 in the lower left of the figure) as for burst E (the next sequence 1–6).

A similar situation holds for bursts F and G, which also bracket a perigee passage and in which peak F in particular shows the characteristic spectral behavior for the onset of all the other bursts: a flattening of the soft X-ray flux while the hard X-ray flux is still rising.

Evidence for burst H is most clearly seen as the shoulder in the light curve (Fig. 1); however, its amplitude is small. Also, burst I at the end of the observation has a small amplitude; this burst is weak and does not show much evidence for delays between soft and hard bands.

In summary, there is evidence for at least 7 bursts (A–G), some of them with relatively large amplitude, during the gradual rise in the first 400 ks of the observation; there may be two other bursts after the peak maximum (H and I) but they are less clear and weaker.

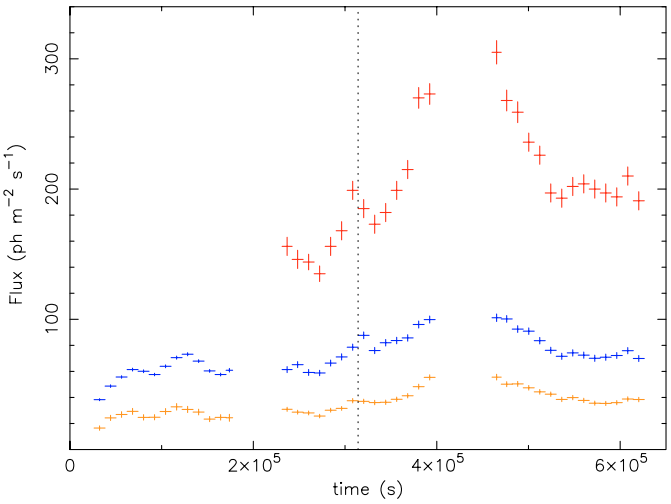

Fig. 2. X-ray light curve of NGC 5548 binned in 12 000 s bins. The fluxes have been corrected for Galactic absorption. From top to bottom: 18–50 Å (soft band), 2–12 Å (hard band) and 18–24 Å. Since the MEG is not sensitive to long wavelength photons, we have no data for the 18–50 Å for the first part of the observation. The dotted vertical line indicates the maximum of the burst in the zeroth order light curve at t = 314.2 ks.

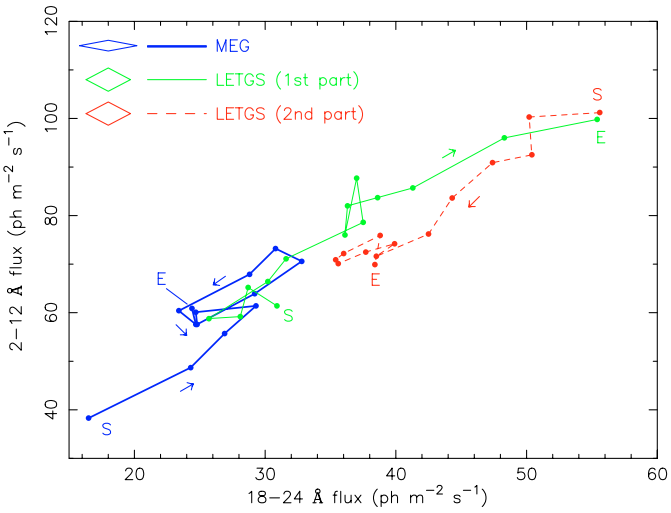

Fig. 3. Hard X-ray (2–12 Å flux) versus soft X-ray (18–24 Å flux) of NGC 5548. Fluxes have been corrected for Galactic absorption. Each data point corresponds to a 12 ks interval. The start and end time bin of each part of the observation are indicated by the "S" and "E" characters. Where needed, arrows indicate the flow of the time sequence. The diamonds in the legend of the figure indicate the error bars on individual data points (which are almost the same for each data-point within each of the three parts of the observation).

We estimated the arrival times of the burst peaks by fitting Gaussians superimposed on a linear rise (Table 1). There is no evidence for true periodicity in the occurrence time of the bursts. However, the interval between the bursts has a characteristic time scale between ~55–80 ks, with a slight tendency to increase starting from burst A to the maximum (around burst F and G). The duration of the bursts (as measured by the *FWHM* from the Gaussian fits) is 52 ± 9, 54 ± 5 and 18 ± 3 ks for A, B and E, respectively.

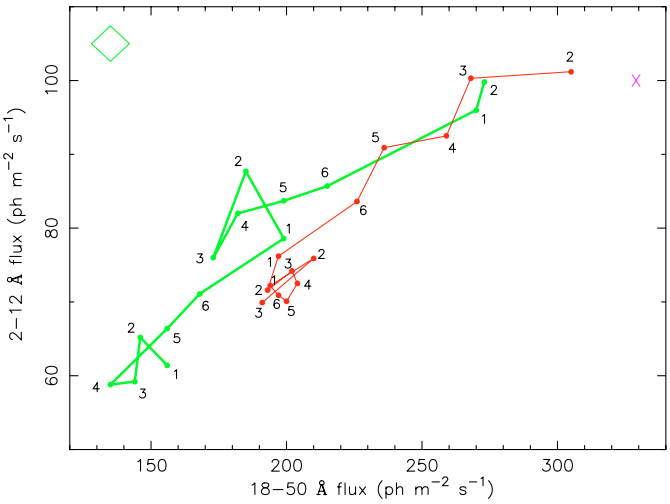

Fig. 4. Hard X-ray (2–12 Å flux) versus soft X-ray (18–50 Å flux) of NGC 5548 (LETGS observations only). Fluxes have been corrected for Galactic absorption. Each data point corresponds to a 12 ks interval. Data points are labeled following the sequence 1, 2, 3, 4, 5 and 6 repeatedly in time (6 times 12 ks is approximately the average time interval between burst peaks in the light curve). The diamond in the upper left corner of the figure indicates the error bars on individual data points (which are almost the same for each data-point in this figure). The "X" in the upper right corner corresponds to the average LETGS spectrum of NGC 5548 during the first observation with *Chandra* of this source in 1999 (Kaastra et al. 2000, 2002).

Table 1. Burst parameters. Here $t_{\rm peak}$ is the time of maximum and $t_{\rm next}$ the time till the next burst maximum.

Burst	$t_{\rm peak}$ (ks)	$t_{\rm next}$ (ks)
A	65 ± 2	58
B	123.0 ± 1.3	>47
C	>170	<61
D	231 ± 7	83
E	314.2 ± 1.1	80
F	394 ± 5	<66
G	<460	>49
H	509 ± 3	105
I	614 ± 4	-

3.2. Continuum spectral variability

The spectrum of NGC 5548 is analyzed in detail by Steenbrugge et al. (2004). Here we summarize their results relevant for the present paper. The continuum is well approximated by the sum of a power law component and a modified blackbody spectrum, a similar model as used by Kaastra & Barr (1989) in their analysis of the EXOSAT data of NGC 5548. In addition, there is a warm absorber that produces both line and continuum absorption. It appears that while the continuum of NGC 5548 is changing, there is no evidence for a significant change in the warm absorber, neither between the HETGS and LETGS observation, nor between the present LETGS observation and the first LETGS observation of December 1999, with the exception of O V. This simplifies our analysis of the continuum variability significantly. The presence of a few

narrow or broadened emission lines (for example the O VII forbidden line) does not affect our present broad-band analysis.

The zeroth order light curve of the LETGS contains no spectral information. However, taking our best-fit spectral model for the LETGS spectrum we estimate that 90% of the zeroth order counts originate from photons between 2–50 Å, with a median photon wavelength of 18 Å. We can get variability information from the first order spectral data, but due to the enhanced background of the HRC-S detector the signal is noisier. Therefore we need to take larger time bins than the 2000 s bins that we used in Fig. 1. We have divided the spectral data of both the HETGS and LETGS in intervals of 12 ks. Utilizing the high spectral resolution of the gratings, we then constructed broad-band light curves which were corrected for the effective area of the instruments and for Galactic absorption ($N_{\rm H} = 1.65 \times 10^{24}$ m^{-2}). Since the MEG effective area drops rapidly at long wavelengths, we restricted the MEG wavelength band to $\lambda < 24$ Å.

Figure 2 shows the absorption-corrected light curves for three bands. Our spectral modeling (Steenbrugge et al. 2004) shows that the hard band (2–12 Å) is entirely dominated by the power law component, while the soft band (18–50 Å) is a mixture of power law and modified blackbody emission. The figure shows that the variability is stronger in the soft band: see for example the sharp rise in soft flux shortly before the maximum at $t = 380$ ks. It is also evident that burst E at $t = 314.2$ (indicated by the dotted line) is delayed in the hard band as compared to the soft band, by about 1 bin (12 ks).

In Fig. 3 we show the relation between soft and hard flux, where for the soft flux we took the 18–24 Å band in order to make use of the MEG data. It is evident that during the HETGS observation and the first LETGS observation the flux in both bands is almost continuously rising, with at least four intermissions in the rise (at approximately the middle and end of the HETGS observation, and at the start and middle of the first LETGS observation). For each of these intermissions first the soft X-ray flux starts decreasing, followed about 1 bin (12 000 s) later by the hard X-ray flux.

This behaviour is even more evident from Fig. 4, where only LETGS data are plotted, so as to replace the 18–24 Å flux by the 18–50 Å flux. The flux in this latter band is on average 5.17 ± 0.05 times larger than in the more restricted band 18–24 Å; the LETGS band shows an almost strictly proportional relation between the flux in both soft bands. Due to the limited statistics it is difficult to estimate the exact delay of the hard band relative to the soft band; however, by locally fitting Gaussians superimposed on a linear rise for each band, using a higher time resolution version of our light curves, we find hard flux delays of 7 ± 3, 5 ± 3, 3 ± 5 and 5 ± 3 ks for bursts A, B, D and E, respectively. The weighted average is 5.4 ± 2.3 ks.

Further we note that our data show the well-known behaviour of the power law component: when the flux increases, the spectrum softens. We have fitted a simple power law to the fluxed, Galactic absorption corrected spectrum in the 2–12 Å band. This "effective" photon index (Γ_{2-12}) is not the true photon index since that is affected by the warm absorber, but given the lack of spectral variability of the warm absorber (see Steenbrugge et al. 2004), it correlates well with the true

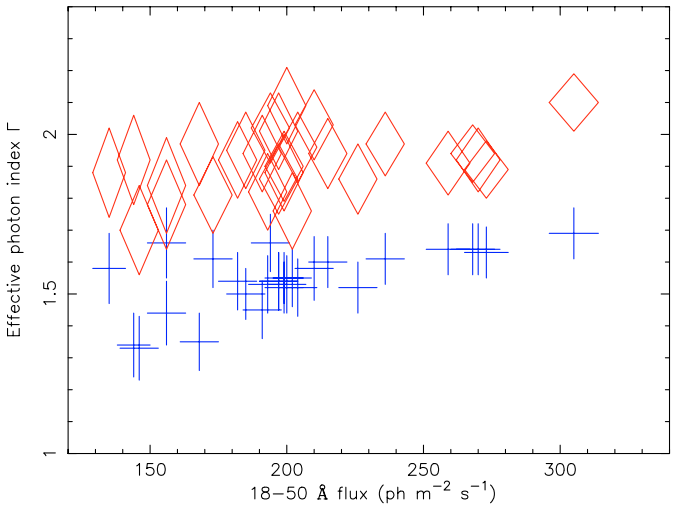

Fig. 5. Effective power law index Γ in the 2–12 Å band (crosses) and 18–50 Å band (diamonds) versus 18–50 Å Galactic absorption corrected flux for the LETGS data.

photon index. This true photon index of the power law component, as deduced from the full spectral fit to the total LETGS spectrum, is 1.88 (Steenbrugge et al. 2004); the time-averaged value of Γ_{2-12} is 1.55. Given the lack of variability of the warm absorber, one may add 0.33 to Γ_{2-12} in Fig. 5 to get the true photon index. Since the continuum in the soft band has a different nature (modified blackbody plus contributions from the hard X-ray power law) the 18–50 Å effective photon index Γ_{18-50} in Fig. 5 cannot be easily transformed into a meaningful physical photon index. It should merely be considered as a convenient parameterisation of the effective spectral slope over this band.

Taking F_{18-50} the observed, Galactic absorption corrected flux in the 18–50 Å band (in units of photons m^{-2} s^{-1}), we find a correlation between Γ_{2-12} and F_{18-50} (Fig. 5). The best fit parameters for a functional relation $\Gamma_{2-12} = a + bF_{18-50}$ are $a = 1.24 \pm 0.12$ and $b = 0.0015 \pm 0.0006$. The relatively low significance of the correlation is mainly due to the size of the errors on the photon index, caused by the relatively small effective area of LETGS at the highest energies. Contrarily, the effective photon index Γ_{18-50} determined the same way but for the 18–50 Å band does not show a strong correlation with the soft X-ray flux (Fig. 5). In this case the best fit parameters for $\Gamma_{18-50} = a + bF_{18-50}$ are $a = 1.74 \pm 0.15$ and $b = 0.0009 \pm 0.0007$. As is well known for NGC 5548 and other Seyfert galaxies, our data do show the well known correlation between photon index Γ_{2-12} and flux F_{2-12} for the power law component alone: the photon index increases from 1.33 at $F_{2-12} = 50$ to 1.66 for $F_{2-12} = 100$ photons m^{-2} s^{-1}.

Thus, the spectral shape in the soft band is less variable than in the hard band, despite the large flux variations in the soft band.

Finally, we investigated the (cross)correlation of our data using the discrete correlation function technique (Edelson & Krolik 1988). In Fig. 6 we show our results. The figure shows a narrow peak with a half-width of about 20–40 ks centered at zero lag. This corresponds to the bursts in the light curve. Despite the fact that for individual bursts the hard X-rays are

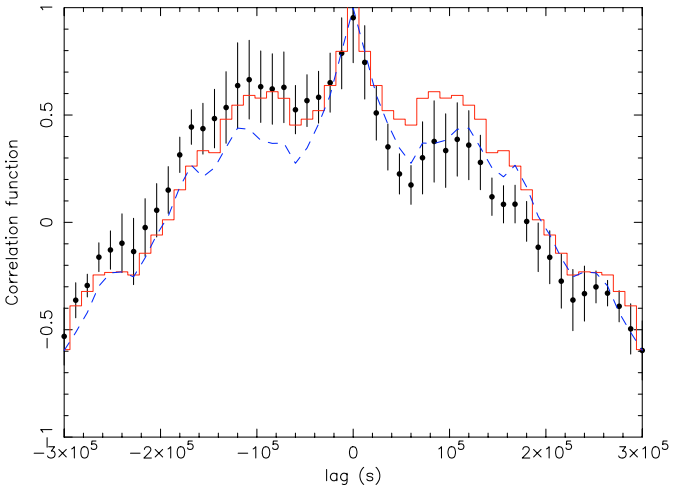

Fig. 6. Discrete correlation function (data points with error bars) of the hard (2–12 Å) with respect to the soft (18–24 Å) band. Positive lags correspond to hard X-rays following soft X-rays. The solid line indicates the discrete autocorrelation function of the soft band, the dashed line the discrete autocorrelation function of the hard band.

delayed with respect to the soft X-rays (as can be seen in Fig. 3), Fig. 6 shows that on longer time scales the hard X-rays tend to lead the soft X-rays. This can be seen from the stronger correlation at a lag of −100 ks as compared to the correlation at a lag of +100 ks. Note that due to the bin size of 12 000 s used in Fig. 6, delays of individual bursts are invisible in that plot. In a higher time resolution correlation plot they also remain invisible due to the addition of noise from the non-burst parts of the lightcurve. Only our hysteresis curves (Figs. 3–4) are able to demonstrate the presence of these delays.

4. Discussion

The lightcurve of NGC 5548 shows several bursts (Fig. 1 and Table 1) with typical intervals between 55–80 ks. There is a slight tendency of longer intervals around the maximum near bursts F and G. The spectra of these bursts show an average delay of the hard X-rays with respect to the soft X-rays of 5.4 ± 2.3 ks.

Such a delay has been seen before in NGC 5548. Kaastra & Barr (1989) found a delay of 4.6 ± 1.2 ks in their correlation analysis of the EXOSAT LE versus ME count rates from two long observations in 1986. Chiang et al. (2003) found a delay of 13 ± 6 ks in their correlation analysis of the 0.5–1 keV ASCA versus the ∼0.14–0.18 keV EUVE Deep Survey (DS) count rates, for their coordinated observations in 1998. The delay of the 2–20 keV RXTE PCA versus EUVE count rate was larger, 34 ± 11 ks, but there is less overlap between both light curves as compared to the ASCA and EUVE data sets.

Interestingly, Dietrich et al. (2001) report an optical flare in NGC 5548 on June 22, 1998 with a rise time of 1.8 ks and decay time less than 3.6 ks. This flare was visible in the U, B, V, R and I bands and had an ampliude of ∼20%. However, no flare is visible in the simultaneous ASCA and RXTE light curves published by Chiang et al. (2003, see their Fig. 1; the peak of the optical flare (JD 2 450 987.37) is 197.2 ks after their reference epoch). Unfortunately the optical flare occurred during a data gap of the simultaneous EUVE observation. Therefore it is hard to say if this optical flare has a physical origin similar to that of the bursts that we observe.

Finally, we note that Haba et al. (2003) found 40% fluctuations in the DS light curve of NGC 5548 in 1996, without simultaneous variations in either the ASCA count rate or spectrum. They conclude that if there is any delay of hard X-rays with respect to soft X-rays, the delay time must be larger than 60 ks. These soft X-ray fluctuations occur at the beginning of their observation during a peak in the X-ray flux, and the DS light curve is remarkably similar to our light curve starting near the maximum (bursts F and G).

We propose the following model for the bursts. We assume that the inner parts of the accretion disk are affected by a thermal instability. This gives rise to the gradual flux increase from the start of our observation to the maximum, around 400 ks after the start of our observation. We assume that there is a rotating hot spot at a distance $R = rGM/c^2$ from the black hole. This spot may fluctuate in intensity and extend during its orbiting of the black hole. Since the maximum emissivity of an accretion disk occurs near $r = 10$, we assume that r is of this order of magnitude.

Numerical simulations of accretion disks (for example Armitage & Reynolds 2003) indicate that hot spots can survive for a few orbital periods.

The rotating hot spot produces soft X-rays by the same processes by which the surrounding parts of the disk emit soft X-rays. The details of this process are not important for our present discussion, but it is clear that some form of reprocessing or Comptonization must occur in the emitting regions, as the shape of the soft X-ray spectrum changes little while its flux is increasing significantly. In our model we assume that the hard X-rays are produced in a different region, by Inverse Compton scattering of the seed photons from the disk and hot spot.

Analytical models for a rotating spot around a black hole were produced by Karas (1996). At distances of $r \sim 10$, the light curve that would be sinusoidal in the non-relativistic case is distorted by Doppler boosting and general relativistic effects. The maximum is boosted while the minimum is flattened in such a way that as a function of orbital phase the light curve is almost flat during half an orbit and has a broad peak during the second half. The maximum occurs at phase 0.6–0.7, when the hot spot is approaching the observer (phase 0.5 is defined as the instant when the spot is behind the black hole). The *FWHM* of the burst is about 30% of the orbital period. The above holds for disk inclination angle $i < 60°$. For larger angles the light curve is dominated by a narrower peak at phase 0.5, caused by focusing of the light by the black hole. However, here we assume that $i < 60°$. From the presence of weak relativistic O VIII and N VII line, Kaastra et al. (2002) derived an inclination angle between 43–54°, in reasonable agreement with the results of Yaqoob et al. (2001) in their re-analysis of ASCA data (31° ± 8°). In Fig. 7 we show an example of the predicted light curve for a non-rotating black hole. The results for a Kerr black hole are very similar.

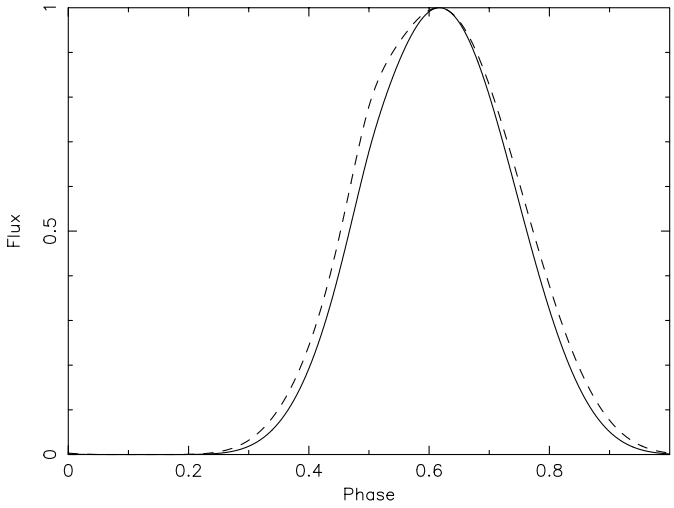

Fig. 7. Predicted pulse profile for a rotating spot around a Schwarzschild black hole, at a distance of $R = 10GM/c^2$ from the black hole. Solid line: inclination 30°; dashed line: inclination 50°. Phase 0.5 is defined as the instant when the spot is behind the black hole. The *FWHM* of both profiles is 0.30 and 0.32, respectively.

The observed interval between bursts of 55–80 ks then corresponds to the orbital period of the hot spot. Irregularities are caused by fluctuations in the emission from the other parts of the disk, as well as fluctuations in brightness and extent of the spot. The expected *FWHM* of the bursts is ∼30% of the orbital period, or between 15–25 ks. The observed duration of the bursts is in agreement with this estimate, in particular for burst E. A somewhat longer duration of bursts A and B near the onset of the instability may be related to the initial formation of the spot over a larger area of the disk.

Peterson & Wandel (2000) estimated the mass of the central black hole in NGC 5548 to be $(5.9 \pm 2.5) \times 10^7\ M_\odot$, based upon reverberation mapping of the broad emission lines. Using this mass range, an orbital period of 55–80 ks corresponds to $r = 8$–18 gravitational radii. In our further estimates, we adopt $r = 10$ and $M = 5.9 \times 10^7\ M_\odot$.

Although the peak luminosity of the bursts reaches some 25% of the underlying rising flux, it should be noted that the burst peaks are highly boosted by Doppler and general relativistic effects. We estimate that the time-averaged power of the bursts is only 5–10% of the total flux. This then implies a typical size of a few gravitational radii for the hot spot.

The expected delay of the hard X-rays with respect to the soft X-rays depends upon the geometry of the emitting regions. There are two factors that may cause a delay. If the Inverse Compton scattering of soft X-ray seed photons occurs much further inward as compared to the location of the hot spot, a delay of order rGM/c^3 or 3000 s may occur. The precise delay depends upon subtleties like inclination angle, distance and geometry of the scattering region and general relativistic effects. The details of such a model are beyond the scope of this paper, however, we note that the expected time delay is of the observed order of magnitude.

The second possible origin of a delay is retardation due to the random walk of the soft X-ray seed photons in the scattering region, as they are being up-scattered to hard X-rays. For typical photon indices and temperatures, optical depths of the order of 2–3 are expected. This produces typical delays of the order of 2–3 times the light travel time through the scattering region. The probable size of the scattering region is less than r, the radius of the soft X-ray emitting region, hence this may give an effect of the same order of magnitude as the time delays due to the separation between hard and soft X-ray emitting regions. Again, the details are very model-dependent. If this scenario holds, then the hard X-ray source has an electron density of order 10^{10} cm^{-3}.

Finally, we propose that around the maximum of the thermal instability, in the middle of our LETGS observation, the hot spot may disappear, as we do not see evidence for strong bursts after this maximum. From the hysteresis plots (Figs. 3 and 4) we see that at the end of the observation the continuum spectral properties differ significantly from the spectral properties during the rise toward the peak, as is evident from the different hard to soft X-ray flux ratio. A similar two state situation has been found in NGC 3783 by Netzer et al. (2003).

Acknowledgements. SRON is supported financially by NWO, the Netherlands Organization for Scientific Research.

References

Armitage, P. J., & Reynolds, C. S. 2003, MNRAS, 341, 1041
Chiang, J., Reynolds, C. S., Blaes, O. M., et al. 2000, ApJ, 528, 292
Crenshaw, D. M., & Kraemer, S. B. 1999, ApJ, 521, 572
Crenshaw, D. M., Kraemer, S. B., Gabel, J. R., et al. 2003, ApJ, 594, 116
Dietrich, M., Bender, C. F., Bergmann, D. J., et al. 2001, A&A, 371, 79
Edelson, R. A., & Krolik, J. H. 1988, ApJ, 333, 646
Haba, Y., Kunieda, H., Misaki, K., et al. 2003, ApJ, 599, 949
Kaastra, J. S., & Barr, P. 1989, A&A, 226, 59
Kaastra, J. S., Mewe, R., Liedahl, D. A., Komossa, S., & Brinkman, A. C. 2000, A&A, 354, L83
Kaastra, J. S., Steenbrugge, K. C., Raassen, A. J. J., et al. 2002, A&A, 386, 427
Kaastra, J. S., Steenbrugge, K. C., Brinkman, A. C., et al. 2003, in Active Galactic Nuclei: from central engine to host galaxy, PASP Conf. Ser., 290, 101
Karas, V. 1996, ApJ, 470, 743
Kriss, G. A., Green, R. F., Brotherton, M., et al. 2000, ApJ, 538, L17
Netzer, H., Kaspi, S., Behar, E., et al. 2003, ApJ, 599, 933
Peterson, B. M., & Wandel, A. 2000, ApJ, 540, L13
Steenbrugge, K. C., Kaastra, J. S., Crenshaw, D. M., et al. 2004, A&A, submitted
Yaqoob, T., George, I. M., Nandra, K., et al. 2001, ApJ, 546, 759